Magnetic Charge and Magnetic Field Distributions in Ferromagnetic Pipe

Huang Xinjing, Chen Shili, Guo Shixu, Zhao Wei, and Jin Shijiu

State Key Laboratory of Precision Measurement Technology and Instrument
Tianjin University, Tianjin, 86-300072, China
1207571368@qq.com, huangxinjing@tju.edu.cn, and shjjin@tju.edu.cn

Abstract ― This paper proposes the equivalent magnetic charge (EMC) method, to analyze the magnetic field presented in ferromagnetic pipe. Distributions of the magnetic charge density on pipes' surface are calculated, and the magnetic field on several measurement lines is predicted using numerical calculation with several different directions of magnetization. The correctness of the analysis results is then validated by the comparison between the results of the ANSOFT and measurement of the magnetic field inside several actual pipes. With the EMC method, it is of great interest to found that when the magnetization direction changes, the radial and axial magnetic field components inside the pipe will shift accordingly. Moreover, the variation law of magnetic field along the axial retains substantially unaltered, and the magnetic field distribution in the pipe is obviously symmetrical with a plurality of extreme points. As a result, the magnetic field distributes evenly if the pipe is long enough.

Index Terms - Magnetization, magnetostatics, magnetic charge, magnetic field, and pipe.

I. INTRODUCTION

In-pipe, pipelines inspection gauge (PIG) represents one of the most popular techniques to detect the pipelines' integrity in oil and gas storage and transportation departments, enabling the early identification of corrosion and early restoration of pipelines before any leak occurs [1]. PIG or other methods as well usually utilize the magnetic field inside or outside the pipelines to discover pipelines' defects and assist in positioning and calculating pipelines' routes [2-4]. Ignoring the distributions of the background magnetic field in the pipelines often leads to inconsistencies between the analysis results of PIG's detection based on the magnetic field inside pipelines and actual pipe disfigurement conditions, inducing additional error to cause great inconvenience to maintain pipelines. Therefore, it is very important to ascertain the distributions of the magnetic field inside the pipelines that serves for the magnetic field measurement and data analyses for PIG, and thus improving the detection accuracy of PIG.

A number of literatures had reported the characteristics of axial uniform magnetization to non ellipsoid using the numerical method, achieving a lot of meaningful results [5-12]. Nakamura et al. [5] gave a detailed description of scalar magnetic potential method for three dimensional analyses of the distributions of the magnetic charge density on the surface of the ferromagnetic material, and analyzed the distributions of the magnetic field around the magnetic poles of the motor. Kobayashi et al. [6] adopted the method proposed in reference [5] to make abundant analyses for cylindrical tubular model applied an axial uniform magnetization, discussing in detail the distribution characteristics of the magnetic charge density on the surface of the ferromagnetic body in cases of different diameter ratios, different aspect ratios, and different magnetic susceptibilities. However, the authors did not involve the distribution characteristics of the magnetic field inside the pipe when applied different directions of magnetization. Chen et al. [13], indicated conversely the distributions of the magnetic charge density on ships' surfaces using the measured magnetic field values at finite points near the ship

Submitted On: Nov. 24, 2012
Accepted On: June 14, 2013

according to the scalar magnetic potential theory, thus predicting the magnetic field generated by the ship at any point in the space accurately. However, this method is affected by the condition number of the calculation matrix and the distribution of the measurement points drastically, making it unreliable and inaccurate in practice. It is therefore very important to develop new methods for accurate magnetic field analyses.

In this regard, this paper presents the equivalent magnetic charge (EMC) method to the magnetic field analyses for pipes to improve the calculation accuracy. With different directions of magnetization of the pipes, we calculate the distributions of the magnetic charge density on the surface of non-axially magnetized cylindrical tubular body and the magnetic field distributions inside the pipe. Simultaneously discrete calculation method used in this paper does not depend on the distribution of measurement points, and the condition number of the calculation matrix is very small. Both of the improvements make the calculation result rather reliable. The present work demonstrates this methodology by comparison between the results of ANSOFT and measurement results of the magnetic field distributions in several actual pipes. The results indicate the correctness of the proposed EMC method, producing a reliable and accurate calculation result for magnetic field analyses.

II. METHOD OF ANALYZING

A. Equivalent magnetic charge theory

For the relative permeability μ, which is finite and homogeneous in the magnetic body, we express the magnetic flux density $\boldsymbol{B}$ in terms of the magnetic field $\boldsymbol{H}$ and the magnetization $\boldsymbol{M}$ as follows,

$$\boldsymbol{B} = \mu_0(\boldsymbol{H} + \boldsymbol{M}) = \mu_0\mu\boldsymbol{H}\ , \tag{1}$$

where

$$\boldsymbol{M} = (\mu - 1)\boldsymbol{H}\ . \tag{2}$$

In three-dimensional magnetostatic problems, usually resultant intensity of magnetic field $\boldsymbol{H}$ at an arbitrary point in space can be expressed by summation of the applied magnetic field $\boldsymbol{H_0}$ and the demagnetizing field $\boldsymbol{H_d}$ as follows,

$$\boldsymbol{H}(\boldsymbol{r}) = \boldsymbol{H}_0(\boldsymbol{r}) + \boldsymbol{H}_d(\boldsymbol{r})\ . \tag{3}$$

The magnetic field intensity at a point ($\boldsymbol{r}$) in space can be expressed as the gradient of the scalar magnetic potential U,

$$\boldsymbol{H}_d(\boldsymbol{r}) = -grad\,U(\boldsymbol{r}) \tag{4}$$

where

$$U(\boldsymbol{r}) = \frac{1}{4\pi}\int_V \frac{-\nabla\cdot\boldsymbol{M}(\boldsymbol{r}')}{|\boldsymbol{r}-\boldsymbol{r}'|}dV' + \frac{1}{4\pi}\int_S \frac{\boldsymbol{M}(\boldsymbol{r}')\cdot\boldsymbol{n}}{|\boldsymbol{r}-\boldsymbol{r}'|}dS'\ . \tag{5}$$

Wherein V represents an occupied space of the ferromagnetic material, S represents the surface of the ferromagnetic material, and $\boldsymbol{n}$ represents the unit outer normal vector at a point $\boldsymbol{r}'$ on the surface of the ferromagnetic material. $\boldsymbol{M}$ is the bulk density of the magnetic dipole moment, i.e., the magnetic polarization intensity.

For uniformly magnetized magnetic media, $\boldsymbol{M}$ is constant, the first term in equation (5) vanishes because of $\nabla\bullet\boldsymbol{M}$ = 0 and only the second term remains. Then, the $\boldsymbol{H_d}$ can be expressed in terms of the surface magnetic charge density $\sigma(\boldsymbol{r})$ as the following integration,

$$\boldsymbol{H}_d(\boldsymbol{r}) = -\frac{1}{4\pi}\int_S grad\,\frac{\sigma(\boldsymbol{r}')}{|\boldsymbol{r}-\boldsymbol{r}'|}dS'\ , \tag{6}$$

where

$$\sigma(\boldsymbol{r}) = \boldsymbol{M}(\boldsymbol{r})\cdot\boldsymbol{n}\ . \tag{7}$$

When the observation point $\boldsymbol{r}$ is taken on the surface of the ferromagnetic material $\boldsymbol{r_s}$, integral equation can be expressed in terms of the integration on the small finite area ΔS including the observation point $\boldsymbol{r_s}$ and the one on the remaining area S' excluding $\boldsymbol{r_s}$, as shown in Fig. 1. Therefore, $\boldsymbol{H_d}(\boldsymbol{r_s})$ can be expressed as follow,

$$\boldsymbol{H}_d(\boldsymbol{r}_s) = \boldsymbol{H}_{d_s}(\boldsymbol{r}_s) + \boldsymbol{H}_{d_o}(\boldsymbol{r}_s) \tag{8}$$

where

$$\boldsymbol{H}_{d_o}(\boldsymbol{r}_s) = -\frac{1}{4\pi}\int_{S'} grad\,\frac{\sigma(\boldsymbol{r}')}{|\boldsymbol{r}_s-\boldsymbol{r}'|}dS'\ . \tag{9}$$

Considering the discontinuity of $\boldsymbol{H_d}(\boldsymbol{r_s})$ at $\boldsymbol{r_s}$ on the interface of the air and the magnetic body, we can get,

$$\left\{\boldsymbol{H}^{(a)}(\boldsymbol{r}_s) - \boldsymbol{H}^{(m)}(\boldsymbol{r}_s)\right\}\cdot\boldsymbol{n} = \sigma(\boldsymbol{r}_s) \tag{10}$$

where

$$\boldsymbol{H}^{(a)}(\boldsymbol{r}_s) = \boldsymbol{H}_0^{(a)}(\boldsymbol{r}_s) + \boldsymbol{H}_{d_s}^{(a)}(\boldsymbol{r}_s) + \boldsymbol{H}_{d_o}^{(a)}(\boldsymbol{r}_s)\ , \tag{11}$$

$$\boldsymbol{H}^{(m)}(\boldsymbol{r}_s) = \boldsymbol{H}_0^{(m)}(\boldsymbol{r}_s) + \boldsymbol{H}_{d_s}^{(m)}(\boldsymbol{r}_s) + \boldsymbol{H}_{d_o}^{(m)}(\boldsymbol{r}_s)\ . \tag{12}$$

Wherein the superscripts (a), (m) denote the air side and the magnetic body side, respectively. Using $\boldsymbol{H}_0^{(a)}(\boldsymbol{r}_s)=\boldsymbol{H}_0^{(m)}(\boldsymbol{r}_s)$, $\boldsymbol{H}_{d_s}^{(a)}(\boldsymbol{r}_s)=\boldsymbol{H}_{d_s}^{(m)}(\boldsymbol{r}_s)$, $\boldsymbol{H}_{d_o}^{(a)}(\boldsymbol{r}_s)=-\boldsymbol{H}_{d_o}^{(m)}(\boldsymbol{r}_s)$, we can get,

$$\boldsymbol{H}_{d_s}^{(m)}(\boldsymbol{r}_s)=-\boldsymbol{H}_{d_s}^{(a)}(\boldsymbol{r}_s)=-\frac{\sigma(\boldsymbol{r}_s)}{2}\boldsymbol{n}. \quad (13)$$

Taking the inner product of equation (12) and $\boldsymbol{n}$, and using equations (2), (7), and (13) we can get,

$$\frac{\sigma(\boldsymbol{r}_s)}{\mu_0(\mu\text{-}1)}=\boldsymbol{H}_0(\boldsymbol{r}_s)\cdot\boldsymbol{n}\text{-}\frac{\sigma(\boldsymbol{r}_s)}{2\mu_0}+\boldsymbol{H}_{d_o}(\boldsymbol{r}_s)\cdot\boldsymbol{n}. \quad (14)$$

Finally, we can get

$$\frac{1}{4\pi}\left(\int_{S'} grad\frac{\sigma(\boldsymbol{r}')}{|\boldsymbol{r}_s-\boldsymbol{r}'|}dS'\right)\cdot\boldsymbol{n}+\left(\frac{1}{2}+\frac{1}{\mu-1}\right)\sigma(\boldsymbol{r}_s)=\mu_0\boldsymbol{H}_0(\boldsymbol{r}_s)\cdot\boldsymbol{n} \quad (15)$$

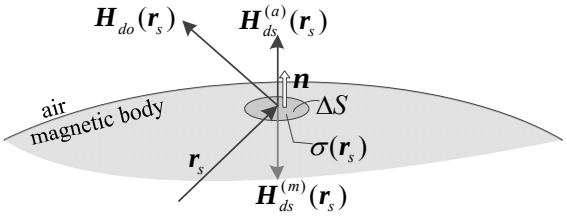

Fig. 1. Magnetic field at a point on the surface of the magnetic body.

B. Discretizing approach

Let us consider the pipe model as shown in Fig. 2. $\boldsymbol{M}$ is the magnetization intensity, $\boldsymbol{M}$ // XOZ plane. The angle between $\boldsymbol{M}$ and OZ axis is α. Inner and outer surfaces and two end surfaces of the ferromagnetic material are divided into N surface elements S_i, i = 1,2,3,…,N, assuming that the magnetic charge density σ_i within each surface element is constant, and then equation (9) can be expressed as equations (16) and (17).

Pipeline is usually made of alloy steel, whose permeability is relatively big [15]. Based on the results from Sakurai et al. [11], we can learn that, when permeability gets larger, the distribution law of the magnetic charge density on the surface of the ferromagnetic material tends to a limit soon in the same mode, but the distribution law keeps consistent. Solving equation (16) we can obtain the distribution of the magnetic charge density on each surface element. For different pipe models, the condition number of the coefficient matrix $\boldsymbol{A}$ of equation (16) is very small, cond $(\boldsymbol{A})\approx 1$.

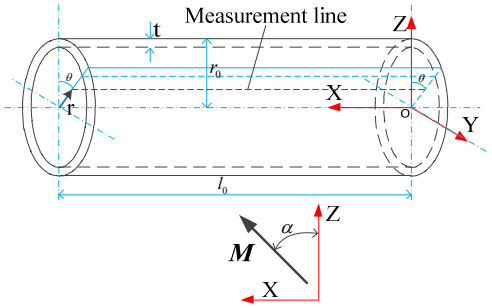

Fig. 2. Pipe model diagram.

$$\begin{pmatrix} \frac{1}{2}+\frac{1}{\mu\text{-}1} & A_{12} & A_{13} & \cdots & A_{1N} \\ A_{21} & \frac{1}{2}+\frac{1}{\mu\text{-}1} & A_{23} & \cdots & A_{2N} \\ A_{31} & A_{32} & \frac{1}{2}+\frac{1}{\mu\text{-}1} & \cdots & A_{3N} \\ \cdots & \cdots & \cdots & \cdots & A_{4N} \\ A_{N1} & A_{N2} & \cdots & A_{N4} & \frac{1}{2}+\frac{1}{\mu\text{-}1} \end{pmatrix} \times \begin{pmatrix} \sigma_1 \\ \sigma_2 \\ \sigma_3 \\ \cdots \\ \sigma_N \end{pmatrix} = \begin{pmatrix} \mu_0\boldsymbol{H}_0\cdot\boldsymbol{n}_1 \\ \mu_0\boldsymbol{H}_0\cdot\boldsymbol{n}_2 \\ \mu_0\boldsymbol{H}_0\cdot\boldsymbol{n}_3 \\ \cdots \\ \mu_0\boldsymbol{H}_0\cdot\boldsymbol{n}_N \end{pmatrix}, \quad (16)$$

where

$$A_{ji,i\neq j}=\int_{S_i}\frac{1}{4\pi}\frac{\boldsymbol{r}_j-\boldsymbol{r}_i}{|\boldsymbol{r}_j-\boldsymbol{r}_i|^3}dS\cdot\boldsymbol{n}_j. \quad (17)$$

C. Calculation method of magnetic field in pipeline

We select a group of measurement points, marked as $P=\{\boldsymbol{r}_i|i=1, 2, \ldots, M\}$. Foregoing divided surface elements here are denoted as $S=\{S_j|j=1, 2, \ldots, N\}$. And then we calculate the magnetic field at each point using equations (18) and (19),

$$\begin{pmatrix} \boldsymbol{H}_1/H_0 \\ \boldsymbol{H}_2/H_0 \\ \cdots \\ \boldsymbol{H}_N/H_0 \end{pmatrix} = \begin{pmatrix} \boldsymbol{C}_{11} & \boldsymbol{C}_{12} & \cdots & \boldsymbol{C}_{1N} \\ \boldsymbol{C}_{21} & \boldsymbol{C}_{22} & \cdots & \boldsymbol{C}_{2N} \\ \cdots & \cdots & \cdots & \cdots \\ \boldsymbol{C}_{M1} & \boldsymbol{C}_{M2} & \cdots & \boldsymbol{C}_{MN} \end{pmatrix} \times \begin{pmatrix} \sigma_1 \\ \sigma_2 \\ \cdots \\ \sigma_N \end{pmatrix} \quad (18)$$

where

$$\boldsymbol{C}_{ij} = \int_{S_j} \frac{1}{4\pi} \frac{\boldsymbol{r}_j - \boldsymbol{r}_i}{\left|\boldsymbol{r}_j - \boldsymbol{r}_i\right|^3} dS \ . \quad (19)$$

III. RESULTS AND DISCUSSIONS

A. Distributions of magnetic charge density on pipes' surfaces

We apply a series of different directions of magnetization to the pipes and calculate the distributions of the magnetic charge density on the surface of the ferromagnetic pipes. The magnetic charge density on each surface element is denoted as σ_{osi}, σ_{isi}, σ_{1ej}, σ_{2ej}, for the outer side, the inner side, the end side1, and the end side2. The mean and standard deviation of $\{\sigma_{osi}/\sigma_{isi}\}$ is calculated and shown in Fig. 3. We can learn that each mean of $\{\sigma_{osi}/\sigma_{isi}\}$ is very close to -1 according to the corresponding directions of magnetization, and the standard deviation is very small. Especially, when the magnetization angle α is less than 80°, the standard deviation of $\{\sigma_{osi}/\sigma_{isi}\}$ is smaller. So it is clear that the magnetic charge density inside and outside pipe is equivalent but opposite for the pipe model. What should be stressed is that pipe cannot be equivalent to a thin model when we analyze its surface's magnetic charge density distribution. We have to calculate all sides of the magnetic charge density of the pipe.

The means of $\{\sigma_{osi},\sigma_{isi}\}$ and $\{\sigma_{1ej},\sigma_{2ej}\}$ are calculated and shown in Fig. 4, using equations (20) and (21). With the magnetization angle α varying from 0° to 90°, the magnetic charge density on the side surfaces becomes larger and larger gradually, while the magnetic charge density on the end surfaces becomes smaller and smaller gradually,

$$\bar{\sigma}_s = \sum_{i=1}^{N_1} \left(\left|\sigma_{osi}\right| + \left|\sigma_{isi}\right|\right) \Big/ 2N_1 \ , \quad (20)$$

$$\bar{\sigma}_e = \sum_{j=1}^{N_2} \left(\left|\sigma_{1ej}\right| + \left|\sigma_{2ej}\right|\right) \Big/ 2N_2 \ , \quad (21)$$

$$\bar{\sigma}_s = k_1 cos\alpha, \bar{\sigma}_e = k_2 sin\alpha, k_2/k_1 \approx 1.5 \ . \quad (22)$$

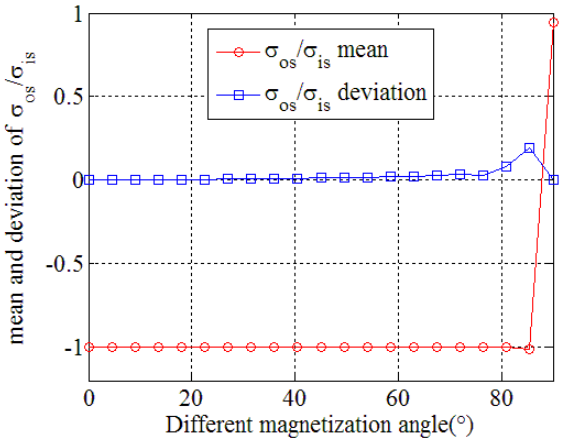

Fig. 3. Inner and outer magnetic charge density contrast on pipe's side surfaces under different directions of magnetization.

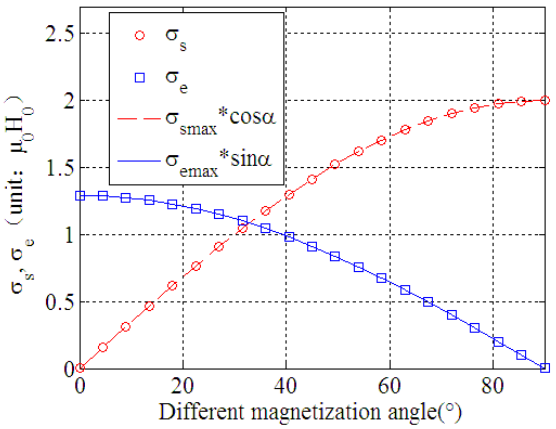

Fig. 4. Contrast of the magnetic charge density on pipe's side and end surfaces under different directions of magnetization.

Some representative results of the foregoing magnetization angles are shown in Figs. 5 (a) - (f) in the form of color intensity maps, which denote the magnetic charge density on the outer surface. As shown in Fig. 5 (a) - (f), when the magnetization direction changes, the distribution of the magnetic charge density changes significantly. However, the magnetic charge density on the outer side surface decreases after the magnetization angle increases. When the magnetization angle α is close to 90°, the circumferential distribution of the magnetic charge density along the pipe has no significant changes, but the axial distribution along the pipe changes significantly, obtaining extremes at the ends of the

pipe. When the magnetization angle α is less than 86°, the circumferential distribution of the magnetic charge density along the pipe changes significantly and shows an obvious periodic variation, obtaining extremes at θ = 0° (+z) and θ = 180° (-z), respectively, but the axial distribution has no significant change.

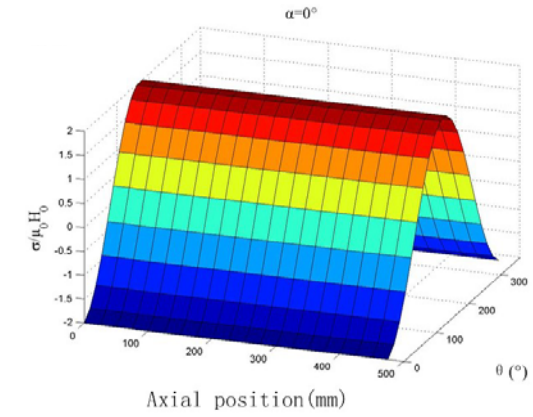

(a)

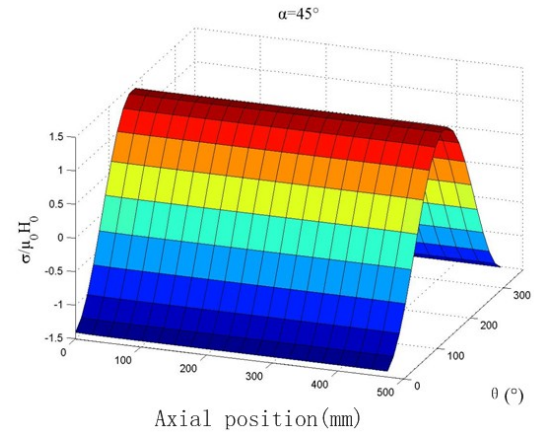

(b)

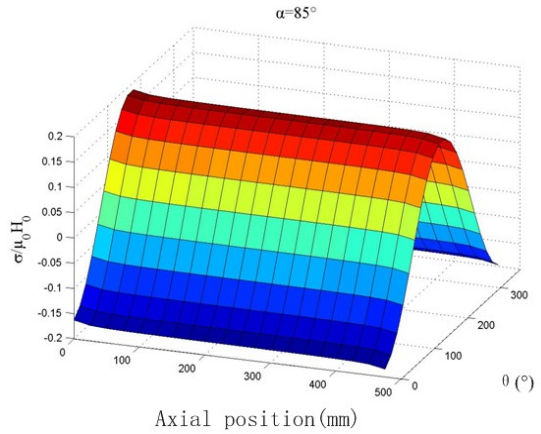

(c)

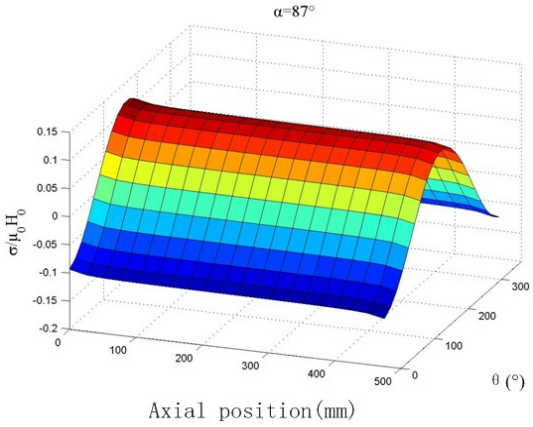

(d)

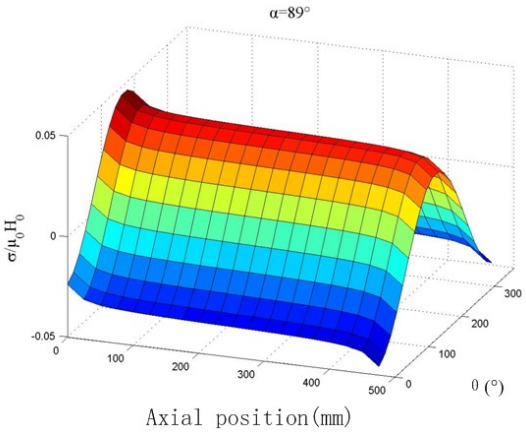

(e)

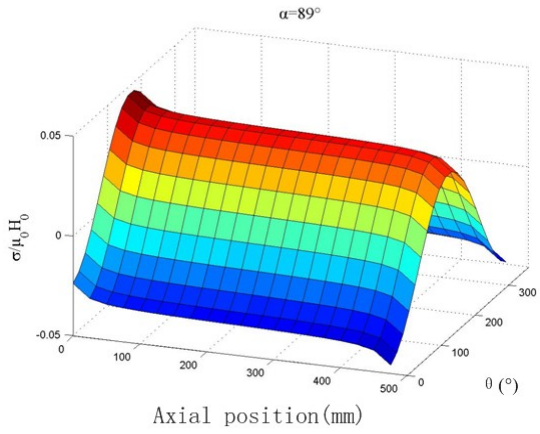

(f)

Fig. 5. Magnetic charge density distributions on pipe's outer side surface under different directions of magnetization.

B. Magnetic field distribution law inside the pipe

The position of the measuring line has no important impact on the magnetic field distribution characteristics as shown in Figs. 6 (a) - (d). For the pipe of l_0= 500 mm, t = 7 mm, r_0 = 100 mm, we take the measuring lines, respectively at r = 0, θ = 0°, r = 0.2 r_0, θ = 0°, r = 0.2r_0, θ = 72°, r = 0.2r_0, θ = 144°. From each graph of Figs. 6 (a) - (d), it is clear that for each magnetization direction, the magnetic field intensity at different measuring lines inside the pipe has no obvious variation either the amplitude or the fluctuation. When the magnetizing angle α increases gradually from 0° to 90°, the axial component H_x of the magnetic field at each measuring line increases gradually, the radial component H_z reduces gradually, but H_y is always very small. The distribution of the magnetic field inside the pipe is obviously symmetrical. H_z shows an even symmetrical distribution all along the axis of the pipe around the median normal plane of the axis of the pipe with only one extreme. When α is very small, H_x shows an odd symmetrical distribution all along the axis of the pipe around the median normal plane of the axis of the pipe with several extremes. When α is big, H_x shows an even symmetrical distribution all along the axis of the pipe around the median normal plane of the axis of the pipe. The distribution of the magnetic field at measuring line r = 0, θ = 0° in the pipe of l_0 = 1500 mm, t = 7 mm, r_0 = 100 mm, is shown in Fig. 6 (e). The results indicate that the magnetic field distribution in the long pipe is similar to that of the short pipe, only with a longer flat portion of the axial and radial magnetic field component. It can be thus expected that the magnetic field will be uniform if the pipeline is very long.

C. Comparison with ANSOFT

In order to confirm the validity of the results above, we perform the finite element analyses for the 500 mm long pipe with the same specification using ANSOFT, a commercial software for electromagnetic simulation. With different magnetization angles of 90°, 45°, and 0°, we analyze the magnetic field distribution inside and outside the pipe, and the simulation results are displayed in the form of magnetic field vector graphic, as shown in Figs. 7 (a) - (c). It can be seen that when the magnetization angle varies, the magnitude and direction of the magnetic field in the XOZ plane inside the pipe obviously changes accordingly. The magnitude and direction of the magnetic field do not change almost inside and outside the pipe far away from both ends of the pipe, basically consistent with the applied magnetization direction. The direction of the magnet field inside the pipe is opposite to the magnetization direction, while the direction of the magnet field outside and far away from the pipe is identical with the magnetization direction. The magnetic field can be approximately assumed uniform inside the pipe far away from the ends and the wall of the pipe, but the magnitude and direction of the magnetic field near to both ends of the pipe has very dramatic changes. We can build a scene in our brain from the magnetic field vector graphic, which presents the distribution of the magnitude and direction of the magnetic field in the axial measurement lines: the direction of B_x changes twice, while the direction of B_z never changes. It can be very easily inferred that all these distribution characteristics are consistent with the analysis results using our method.

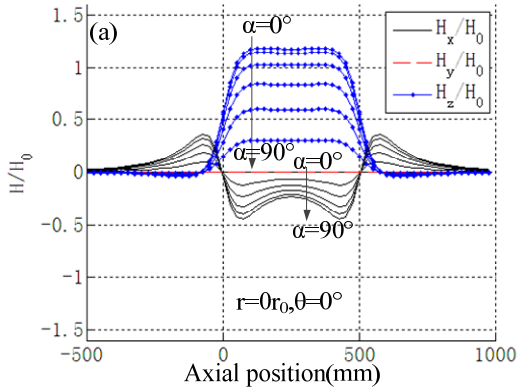

(a)

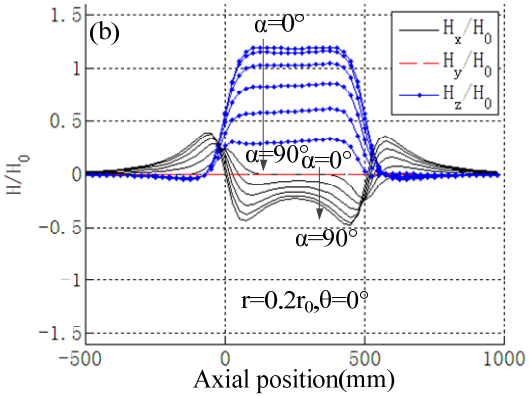

(b)

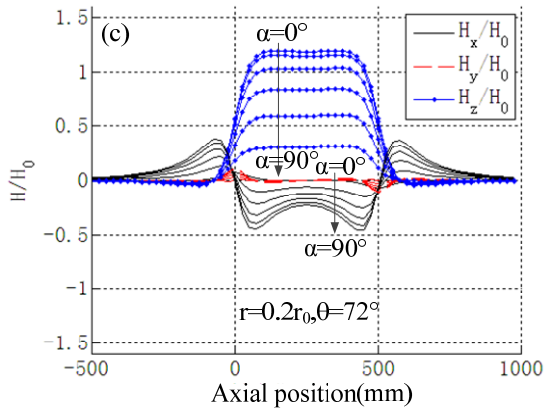

(c)

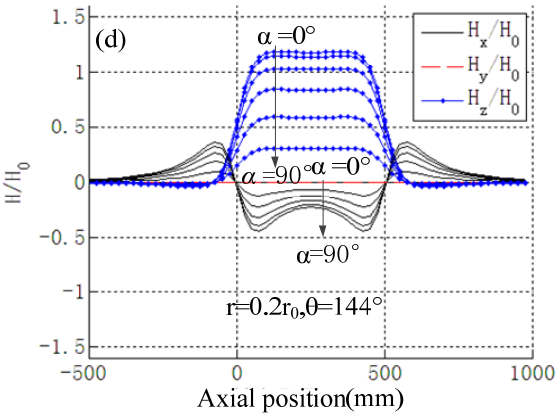

(d)

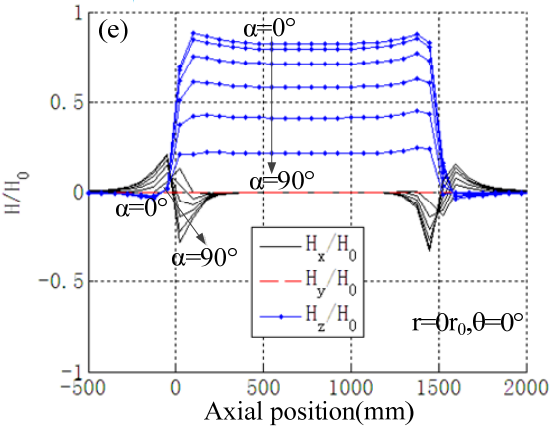

(e)

Fig. 6. Magnetic field distributions in different pipes under different directions of magnetization; α = 0°, 15°, 30°, 45°, 60°, 75°, 90°; r_0 = 100 mm, t = 7 mm, (a)-(d) l_0 = 500 mm and (e) l_0 = 1500 mm.

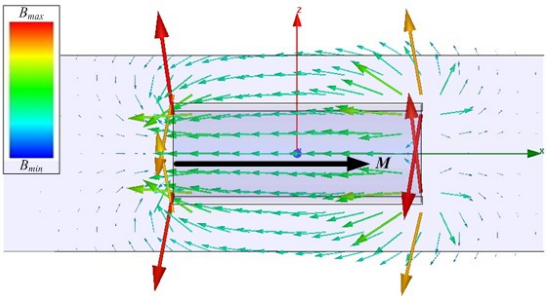

(a)

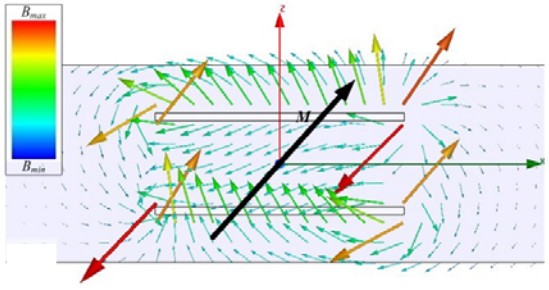

(b)

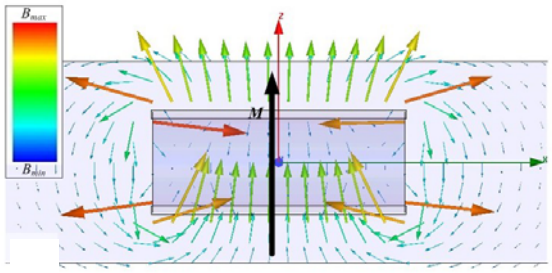

(c)

Fig. 7. Simulation results of ANSOFT.

D. Experiments

For the purpose of verifying the correctness of the analyses above, we measure the magnetic field distribution in several sections of the pipes using the experimental apparatus shown in Fig. 8. Guide rail is parallel to the pipe's axis and goes through the pipe. The slider moves along the pipe's axis as uniform as possible, carrying the magnetic sensor HMC2003. The magnetic induction intensity ***B*** output by the magnetic sensor is collected in real time by the USB4431 data acquisition card. The sensor HMC2003 is a magneto-resistive sensor, which is produced by the Honeywell Company. It has the following features: three-axis sensing, 4nT resolution, 1V/100uT sensitivity, and 0.5V-4.5V voltage output. The data acquisition card

USB4431 is produced by the national instruments (NI) company. It has the following features: four analog inputs, 24 bits resolution, 102.4 ksps synchronous sampling rate, and input range of ± 10 V, one analog output. The data acquisition software LabView is also developed by the NI Company. The pipe's specifications are shown in Table I. The experiment data is shown in Figs. 9 (a)-(d).

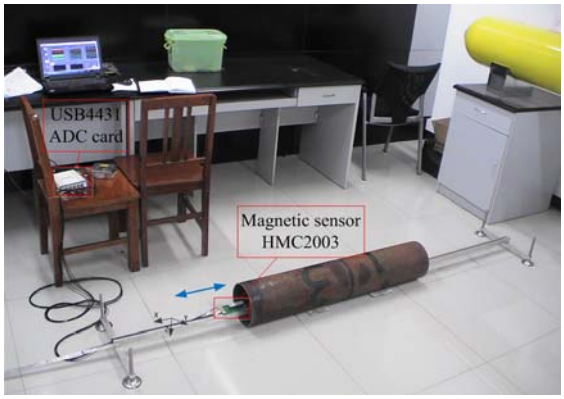

Fig. 8. Experiment equipment.

Table I: Specifications of experimental pipes.

Parameters	Pipes 1, 2	Pipe 3
Length l_0/mm	500	1500
Radius r_0/mm	100	100
Thickness t/mm	7	7
Material	20#	20#

The intensity of the magnetization has little impact on the distribution characteristics of each magnet field component along the axial measurement lines inside the pipe. When the intensity of the magnetization changes with the magnetization direction kept constant, all components of the magnet field are only multiplied by the same scale factor. Therefore, we do not care much about the intensity of the magnetization, and we have not normalized the measured magnetic field inside the pipe to the magnetization magnetic field. There is only a difference of a coefficient between the magnetic induction density $\boldsymbol{B}$ and the magnetic field $\boldsymbol{H}$. Anyway, it can also confirm the correctness of our analyses above by comparing the relative amplitude of the measured magnetic induction density with that of the theoretical analyses above.

For short pipes, we can learn that the measured three-dimensional magnetic field is very consistent with the theoretical analysis results by the comparison of Fig. 9 (a) and Figs. 6 (a)-(d) (when α = 60°). In comparison of the results presented in Fig. 9 (b) and Figs. 6 (a)-(d), it is clear that the actual measured B_x component and B_z component are basically consistent with that of theoretical analysis results. But B_y is not zero, this is due to the inconsistent thing between sensor's sensitive axes y, z and reference axes y, z in the coordinate system as shown in Fig. 2. Therefore, we integrate radial components B_y and B_z into one component, as shown in Fig. 9 (c). The composited magnetic field is very consistent with the results as shown in Figs. 6 (a)-(d) (when α = 30°). In comparison of Fig. 9 (d) and Fig. 6 (e) (when α = 45°), we can learn that the measured B_x component is basically consistent with the theoretical analysis results, and the B_y component and B_z component are very consistent with the theoretical analysis results.

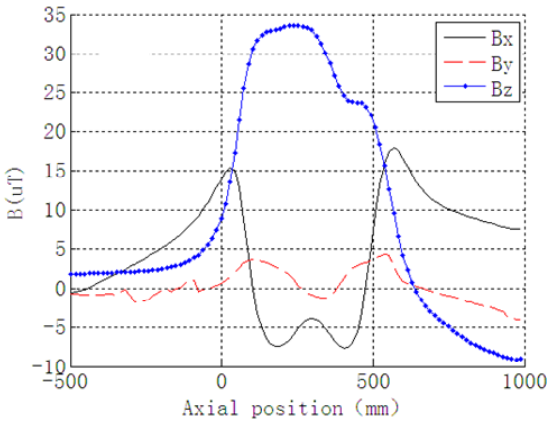

(a)

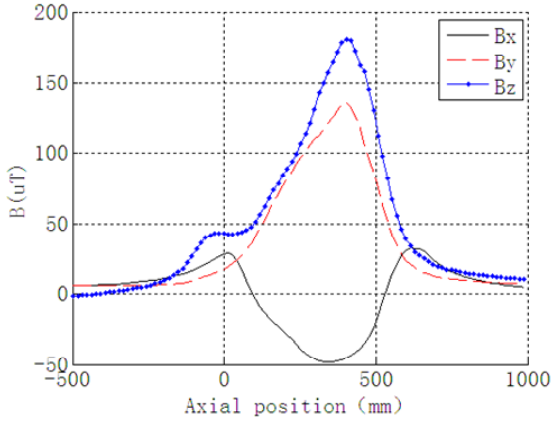

(b)

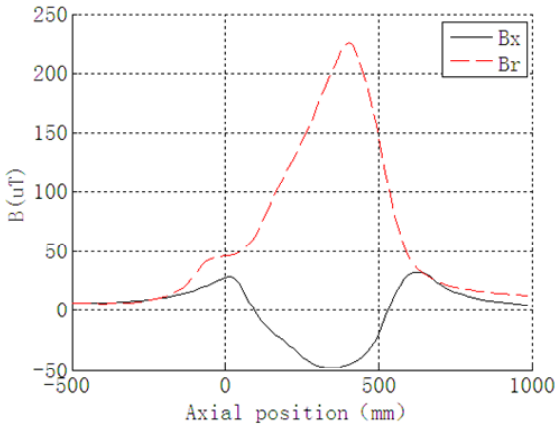

(c)

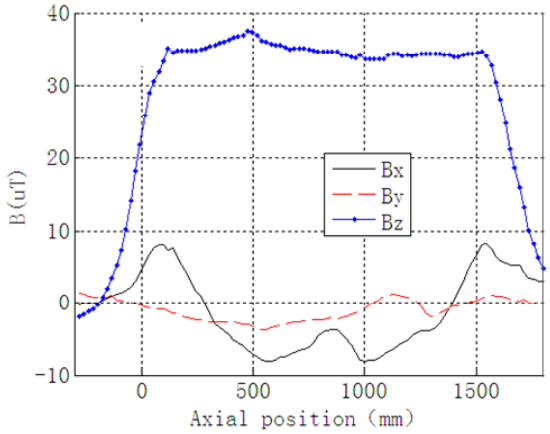

(d)

Fig. 9. Measured magnetic induction intensity inside pipes; (a)-(c) l_0 = 500 mm and (d) l_0 = 1500 mm.

IV. CONCLUSION

In this paper, the EMC method is used to analyze the magnetic field inside pipes. We calculate the distributions of the magnetic charge density on the surface of a non-axially magnetized cylindrical tubular body and the inner magnetic field distributions with different directions of magnetization applied to the pipe. By comparison with the simulation results of ANSOFT and measurement of the magnetic field distributions within several actual pipes, we validate the correctness of the analyses in this paper. Theoretical analyses and experimental results show that: the axial magnetic field distribution in the pipe is obviously symmetrical and with a plurality of extreme points; when the magnetization direction varies, the axial component and radial components of the magnetic field inside the pipeline will shift, but the magnetic field variation law along the axial retains substantially unchanged; the magnetic field will be uniform if the pipe is long enough.

The research results can be used to evaluate the background magnetic field distribution in the pipelines, and contribute to the magnetic field measurement strategies and the data analyses for PIG. For example, if we know the distribution characteristics of the background magnetic field inside the pipelines, we can make use of the mutation of the magnetic field near the girth weld to identify the weld to correct the mileage measurement error of the in-pipe detector, utilize the abnormal magnetic field to estimate the pipeline damage, or adopt the magnetic field in the pipelines to calculate the angle between the geomagnetic field and pipeline to determine the pipeline route. It is also obvious that considering the background magnetic field distributions in the pipelines can make it closer between PIG's detection analysis results based on the magnetic field inside the pipelines and the actual pipelines' disfigurement conditions, thus reducing calculation error and improving the detection precision.

REFERENCES

[1] Y. Zhou, H. R. Dong, Z. G. Zhou, and H. Xie, "The development of in-line inspection technology of oil and gas pipeline," *China Petroleum Machinery*, vol. 39, no. 3, pp. 74-77, 2011.

[2] W. Zhao, Z. M. Zeng, S. L. Chen, Y. Zhang, and S. J. Jin, "Analysis and experimental study of the characteristic of geomagnetic field inside pipeline," *Chinese Journal of Scientific Instrument*, vol. 33, no. 7, pp. 1556-1560, July 2012.

[3] S. I. Sheikh, H. A. Ragheb, K. Y. Alqurashi, and I. Babelli, "A microwave technique for detecting water deposits in an air flow pipelines," *Applied Computational Electromagnetics Society Journal*, vol. 25, no. 7, pp. 647-651, July 2010.

[4] F. Deek and M. El-Shenawee, "Microwave detection of cracks in buried pipes using the complex frequency technique," *Applied Computational Electromagnetics Society Journal*, vol. 25, no. 10, pp. 894-902, Oct. 2010.

[5] S. Nakamura, T. Nomura, and M. Iwamoto, "Three dimensional analysis of leakage field in a power transformer," *IEE Trans. Japan*, vol. 96, no.

5, pp. 443-450, 1976.

[6] M. Kobayashi and H. Iijima, "Surface magnetic charge distributions of cylindrical tubes," *IEEE Transactions on Magnetics*, vol. 32, no. 1, pp. 270-273, Jan. 1996.

[7] M. Kobayashi and Y. Ishikawa, "Surface magnetic charge distributions and demagnetizing factors of circular cylinders," *IEEE Transactions on Magnetics*, vol. 28, no. 3, pp. 1810-1814, May 1992.

[8] K. Ozaki, M. Kobayashi, and G. Rowlands, "Surface magnetic charge distribution of a long, thin cylinder and its edge singularity," *IEEE Transactions on Magnetics*, vol. 34, no. 4, pp. 2185-2191, July 1998.

[9] M. Kobayashi, Y. Ishikawa, and S. Kato, "Magnetizing characteristics of circular cylinders in perpendicularly applied magnetic field," *IEEE Transactions on Magnetics*, vol. 32, no. 1, pp. 254-258, Jan. 1996.

[10] S. Kato and M. Kobayashi, "Magnetic charge densities around edges of circular cylinders," *IEEE Transactions on Magnetics*, vol. 32, no. 3, pp. 1880-1887, May 1996.

[11] S. Sakurai, N. Soda, M. Kobayashi, and G. Rowlands, "Geometries with the demagnetizing energy independent of the direction of magnetization," *IEEE Transactions on Magnetics*, vol. 43, no. 3, pp. 982-991, March 2007.

[12] N. Soda, M. Kobayashi, and G. Rowlands, "Charge densities and inclination angles of magnetization on various surfaces of rotational symmetry," *IEEE Transactions on Magnetics*, vol. 40, no. 4, pp. 1763-1768, July 2004.

[13] J. Chen and X. W. Lu, "A method for magnetic field prediction caused by naval vessels using magnetic charge distribution," *ACTA Physica Sinica*, vol. 58, no. 6, pp. 3839-3843, June 2009.

[14] S. X. Wang and Y. X. Jia, "Equivalent magnetic monopoles model for calculation of magnetic field," *Journal of Taiyuan Heavy Machinery Institute*, vol. 11, no. 3, pp.85-87, 1990.

[15] Q. Bing, "Quick reference of commonly used steel's magnetic characteristic curve," *Beijing: China Machine Press*, pp. 17-18, 2004.

Huang Xinjing was born on April 13, 1987, in the Henan province of China. He received his B.Sc. degree in the Tianjin University where he is currently working toward his Ph.D. degree. His current research interests involve the distribution characteristics of the magnetic field in the pipeline and its application in the detection and location of pipeline damage.

Chen Shili, was born in the Hubei province, China, in 1973. He received his B.Sc. and Ph.D. degrees both from the College of the Precision Instrument & Opto-electronics Engineering of Tianjin University, in 1997 and 2003, respectively. Here he is currently an Associate Professor. His research interests include ultrasonic phased array inspection, novel online in-pipe detector, pipeline safety warning, etc.

Jin Shijiu received his B.Sc. and M.Sc. degrees in 1970 and 1981, respectively, both from the College of Precision Instrument & Opto-electronics Engineering of the Tianjin University, where he is now a Professor, and a doctoral supervisor. His main research area covers detection technology and equipment, automatic measurement and control system, system integration and optimization, etc.